Journal of Applied Physics

RESEARCH ARTICLE | APRIL 24 2023

Study of device characteristics of intrinsic Josephson junction terahertz emitters related to annealing conditions of the crystals

S. Nakagawa ✉; T. Shizu; T. Imai; ... et. al

Journal of Applied Physics 133, 163904 (2023)
https://doi.org/10.1063/5.0137830

Journal of Applied Physics ARTICLE scitation.org/journal/jap

Study of device characteristics of intrinsic Josephson junction terahertz emitters related to annealing conditions of the crystals

Cite as: J. Appl. Phys. **133**, 163904 (2023); doi: 10.1063/5.0137830
Submitted: 6 December 2022 · Accepted: 6 April 2023 ·
Published Online: 24 April 2023 · Corrected: 2 May 2023

S. Nakagawa,[1,2,a)] T. Shizu,[1] T. Imai,[1] M. Nakayama,[1,2] J. Kim,[1] H. Minami,[1,3] K. Kadowaki,[1] M. Tsujimoto,[4] H. Nakao,[5] H. Eisaki,[2] S. Ishida,[2] T. Mochiku,[6] Y. Hasegawa,[7] and T. Kashiwagi[1,3]

AFFILIATIONS

[1]Graduate School of Pure and Applied Sciences, University of Tsukuba, 1-1-1 Tennodai, Tsukuba, Ibaraki 305-8573, Japan
[2]Research Institute for Advanced Electronics and Photonics, National Institute of Advanced Industrial Science and Technology (AIST), 1-1-1 Umezono, Tsukuba, Ibaraki 305-8568, Japan
[3]Division of Materials Science, Institute of Pure and Applied Sciences, University of Tsukuba, 1-1-1, Tennodai, Tsukuba, Ibaraki 305-8573, Japan
[4]Research Center for Emerging Computing Technologies, National Institute of Advanced Industrial Science and Technology (AIST), Central2, 1-1-1 Umezono, Tsukuba, Ibaraki 305-8568, Japan
[5]Photon Factory, Institute of Materials Structure Science, High Energy Accelerator Research Organization (KEK), Tsukuba, Ibaraki 305-0801, Japan
[6]National Institute for Materials Science (NIMS), 1-2-1 Sengen, Tsukuba, Ibaraki 305-0047, Japan
[7]The Institute for Solid State Physics, The University of Tokyo, 5-1-5 Kashiwa-no-ha, Kashiwa, Chiba 277-8581, Japan

[a)]**Author to whom correspondence should be addressed:** nakagawa.shungo.su@alumni.tsukuba.ac.jp

ABSTRACT

We fabricated terahertz (THz) wave emitters from high-temperature superconductor $Bi_2Sr_2CaCu_2O_{8+\delta}$ (Bi2212) single crystals annealed under oxygen gas (O_2) flow and nitrogen gas (N_2) flow conditions. To better understand the annealing effects of the crystal for the device, we evaluated both device properties and a *c*-axis lattice constant using x-ray diffraction. Compared to the N_2-annealed sample, the O_2-annealed sample shows higher critical current in the current–voltage characteristics and no clear emission. In addition, multiple hysteresis loops were observed above 75 K. Based on the x-ray diffraction measurements, it is suggested that the presence of multiple hysteresis loops observed in the I–V characteristics of the O_2-annealed sample is caused by the existence of layers that have varying levels of oxygen content along the *c*-axis direction of the crystal. The formation of these layers is attributed to the deposition process of metallic thin films during the device fabrication procedure. This result indicates that the Bi2212 crystal surface of the O_2-annealed sample is more sensitive than that of the N_2-annealed one. The information is useful for preparing the Bi2212 crystals for THz-wave emitting devices.

I. INTRODUCTION

High-frequency wireless connection tools, such as cellular phones, have become necessities in our recent lives. These communication tools have been developed step by step so as to achieve higher-speed communication with a larger amount of data, lower delay time, multi-connection, etc. Toward these objectives, THz waves are regarded as promising frequency regions. Furthermore, numerous applications that utilize THz waves, including non-destructive imaging and sensing, astronomy, biological research studies, and medical diagnosis, are currently under development.[1–3]

As for the THz emitters, semiconducting solid-state devices, such as resonant tunneling diodes (RTDs)[4–7] and quantum cascade lasers (QCLs),[8–12] have been extensively developed. As for RTDs, the sub-mW level of output power is achieved. However, there are

technical difficulties to generate higher output power above 1 THz.[13–15] QCLs have good output power characteristics reaching as high as 138 mW at 4.4 THz[9] and can generate frequencies ranging from 1.2 to 5.4 THz. However, since the operating maximum temperatures of QCLs are restricted by $T_{max}(K) = (h/k_B)f \sim 50f$ (THz), where h is Planck's constant and k_B is Boltzmann's constant,[8] a low-temperature operation is required in order to produce the THz waves with frequency around 1 THz.[10] Recently, for the room temperature operation of QCLs, difference-frequency generation QCL techniques have been developed.[16–18]

We have developed THz emitters by using single crystals of a high-temperature superconductor $Bi_2Sr_2CaCu_2O_{8+\delta}$ (Bi2212). Bi2212 is composed of alternating stacks of the insulating Bi_2O_2 layers and the superconducting CuO_2 layers along the c-axis. This stacking structure results in forming intrinsic Josephson junctions (IJJs).[19–21] Accordingly, when a dc voltage is applied across a small mesa structure made of a Bi2212 single crystal, THz waves are emitted (Bi2212-THz emitter)[22] due to the AC Josephson effect.[23] The mesa structure also functions as an electromagnetic (EM) cavity, with the standing wave modes depending upon its geometrical shape. When the frequency of the generated THz current matches the resonance frequency of a cavity mode, EM waves in the THz region are strongly enhanced.[22,24–26]

According to previous studies, the Bi2212-THz emitters produce THz waves with radiation frequencies ranging from 0.3 to 2.4 THz.[27–30] The maximum output power was approximately 30–100 μW from a single mesa device.[27,29,31–33] It was reported that a 0.6 mW level of output power was achieved by synchronizing three mesa structures.[33] In addition, emissions ranging from $1 \sim 11$ THz were reported, from thinner and narrower rectangular Bi2212 devices.[34] Recently, it was shown that the polarization of the EM waves can be controlled.[35–37] Information about the developments of the Bi2212-THz emitters can be obtained from review articles.[38–42]

To date, extensive research has significantly improved device structures and their fabrication processes. On the other hand, while it is known that material properties of crystals [superconducting transition temperature (T_c), chemical composition, hole-doping, etc.] have an influence on device properties,[43] the detailed relevance of these properties is not yet understood. For example, it is empirically believed that slightly under-doped crystals [e.g., annealed at 600°C with 0.1% oxygen gas (O_2)/99.9% argon gas flow] are better for device use.

In this work, in order to obtain a better understanding of the device characteristics from a materials point of view, we attempted to evaluate the electric and material properties of the Bi2212 crystal chips (Bi-chips). Specifically, Bi-chips were fabricated from crystals annealed under two typical conditions, under N_2 flow and under O_2 flow. The c-axis lattice constants were evaluated using x-ray diffraction experiments with synchrotron radiation, depending on the annealing conditions. We evaluated the device characteristics of the samples, based on the current–voltage characteristics and emission characteristics, depending on the applied bias voltages. As a result, the material properties have helped to gain a better understanding of the device's electrical characteristics. The information is useful for preparing the Bi2212 crystals for THz-wave emitting devices.

II. SAMPLE PREPARATIONS AND EXPERIMENTAL METHODS

Bi2212 single crystals were grown using the floating zone method. The details of the crystal growth are described in Ref. 44. The crystals were cut into $\sim$3 mm^2 squares. Then, to adjust the excess oxygen content of these crystals, they were annealed for 4–6 days either under O_2 gas flow at 400°C with a flow rate of 0.10 l/min or under N_2 gas flow at 600°C with a flow rate of 1.0 l/min. In the case of an N_2 gas flow, oxygen content was monitored using an oxygen analyzer (YOKOGAWA, OX400) and was found to be less than 1 ppm. At the end of annealing, the crystals were quenched. The main purpose of the post-annealing is to tune the hole-doping.[45,46]

To fabricate the Bi-chips from the crystals, the following wet etching method, established in our previous study,[47,48] was used. First, both sides of the crystals were cleaved to prepare thin single-crystal plates with a thickness of 3–5 μm. Then, silver and gold were deposited on both sides of the crystals. The total thickness of this metal film was about 10 nm. Then, the photolithography techniques were used to create a mask pattern in the shape of $80 \times 200\,\mu$m^2 rectangles on the surface of the crystals. The crystals were then processed into the shape of the Bi-chip by the wet etching method.

In the following, the Bi-chips prepared using O_2- and N_2-annealed crystals are referred to as Bi-chip-O_2 and Bi-chip-N_2, respectively. The dimensions of the obtained Bi-chips were about $190 \times 70\,\mu$m^2 for Bi-chip-O_2 and about $180 \times 60\,\mu$m^2 for Bi-chip-N_2.

θ–2θ scans using x-ray diffraction were performed to study the distribution of the c-axis lattice constants of the crystals that were processed into Bi-chips. A four-circle diffractometer was used at BL-4C in Photon Factory, High Energy Accelerator Research Organization (KEK). The beam shape at the sample position is elliptic with 0.6 mm vertical and 0.8 mm horizontal. The incident x-ray energy was set to be 8.8 keV with a Si(1 1 1) double-crystal monochromator. In the present measurements, we are able to evaluate the precise distribution of the lattice constants on the order of 10^{-2} Å for micrometer-sized samples.

Some of the fabricated Bi-chips were assembled as Bi2212-THz emitters using a sandwich structure developed by our group.[29,40] In this structure, the Bi-chips are sandwiched between two sapphire substrates. The diameter and thickness of the substrate are 7 and 0.5 mm, respectively. The electrodes were constructed on the top surface of the substrates through sputtering of Cr and Au. The devices were mounted on a cold finger of a helium-flowing cryostat (Oxford Instruments, CF1104) equipped with an optical window. The electrical characteristics of the devices were measured using the conventional two-terminal method. An InSb thermal electron bolometer (HEB, QMC Instruments, QFI/2BI) was used to detect the electromagnetic waves from the devices.[29,40,49]

It is noted that the Bi-chips used for the x-ray diffraction measurements and the device characteristics measurements were different; however, they were made simultaneously from the same single crystal fragment.

III. RESULTS AND DISCUSSION

We measured the temperature dependencies of the magnetic susceptibility of the prepared samples to evaluate the amount of

hole-doping. Figure 1 shows the temperature dependence of the normalized susceptibility of the samples annealed under two different conditions. For the measurements, the single crystals with ~2 mm^2 were used. The magnetic fields of 5 Oe were applied parallel to the *c*-axis of the crystals.

The transition temperature onset, $T_{c\ onset}$ [defined by a crossing point between two extrapolation lines of the normal state and the diamagnetic transition curve in the field cooling (FC) measurement] was 84.2 K for the N_2-annealed crystal and 83.1 K for the O_2-annealed crystal, respectively. It is noted that other Bi2212 single crystals prepared in the same way exhibited maximum T_c of approximately 89 K after specific heat treatment. From these results, it was determined that the N_2 crystal is under-doped and the O_2 crystal is over-doped.

Figure 2 shows the θ–2θ scans of two Bi-chips at around 0 0 20 reflections. Optical photographs of the Bi-chips glued on metallic plates by varnish are also displayed in Fig. 2. The θ–2θ scans shown in Fig. 2 have two obvious differences. First, the θ–2θ scan of the Bi-chip-O_2 shows two peaks at $2\theta = 54.36°$ and 54.51°, while the θ–2θ scan of the Bi-chip-N_2 shows a single peak at $2\theta = 54.30°$. Second, the positions of the two peaks observed in the Bi-chip-O_2 are higher than the peak position observed in the Bi-chip-N_2. According to the peak positions of the θ–2θ scan of the Bi-chip-O_2, the estimated lattice constants of the *c*-axis are 30.77 Å (at $2\theta = 54.51°$) and 30.84 Å (at $2\theta = 54.36°$). In the case of the Bi-chip-N_2, the estimated lattice constant of the *c*-axis is 30.88 Å.

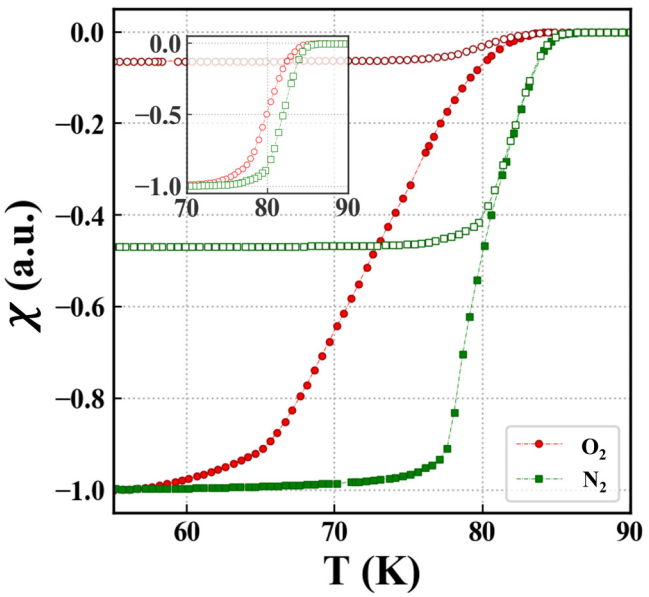

FIG. 1. Temperature dependence of normalized magnetic susceptibilities for two single crystals annealed under different atmospheric conditions. The observed data were normalized to be −1 by using the susceptibility data obtained at the lowest temperature. The filled and open symbols indicate the zero field cooling and field cooling measurements, respectively. The inset displays a magnification plot around T_c for the field cooling measurements. The data shown in the inset were also normalized to be −1 by using the susceptibility data obtained at the lowest temperature of the field cooling measurements.

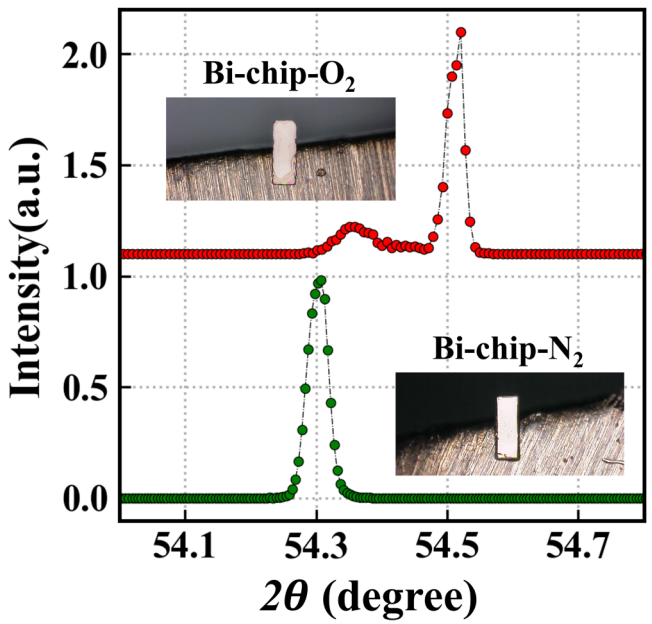

FIG. 2. The θ–2θ scan plots for the Bi-chip-O_2 and the Bi-chip-N_2 around 0 0 20. The optical photographs of the Bi-chips are also displayed near the curves.

It is known that the *c*-axis lattice constant of Bi2212 shrinks with increasing oxygen content.[50,51] The lattice constant values of 30.88 Å and 30.77 Å are generally consistent with previous studies for under-doped and over-doped crystals, respectively.[52] It is noted that nonstoichiometric compositions of Bi and Sr in the crystals also affect the lattice constant.[53] The present results indicate that Bi-chip-O_2 contains two kinds of layers with different hole concentrations, and both layers are more hole-doped compared with Bi-chip-N_2.

To clarify the origin of the double peaks in the O_2-annealed crystals, we also measured the θ–2θ scans of bulk (~2 mm^2 size) Bi2212 single crystals annealed with O_2. Figure 3 shows the results of an x-ray diffraction experiment of the samples. The measurement system was the same as the one used for the Bi-chips.

As shown in Fig. 3, the surface of the sample with the deposited metal film was cleaved and removed. θ–2θ scans were performed both before and after cleaving to evaluate the crystal state. As with the Bi-chip, the total thickness of the Ag and Au deposited metal thin film is about 10 nm. The intensity of the scan data was normalized by the maximum value and plotted on a logarithmic scale.

A low-angle side peak is present in the crystals before cleavage. The peak is not naturally observed in crystals before metal deposition, but it can be obtained with high reproducibility in deposited O_2-annealed crystals. Furthermore, the peak is observed not only in Ag and Au deposition but also in Au- or Ag-only deposition, Au sputtering, and Ar ion sputtering. On the other hand,

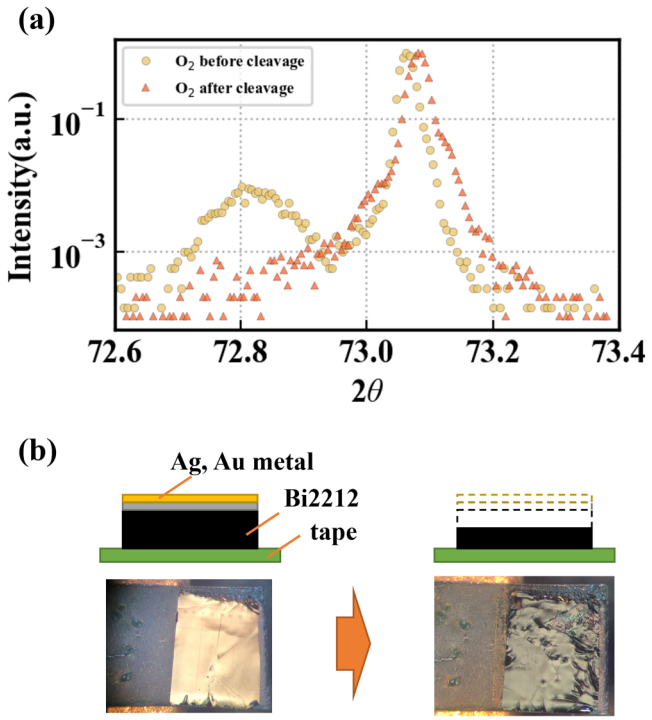

FIG. 3. (a) The θ–2θ scans around 0 0 26 of a Bi2212 bulk single crystal. This crystal has a total of about 10 nm of Ag and Au deposited on the surface. Measurements were taken before and after the surface cleavage. (b) Schematic image and optical photographs of the samples evaluated.

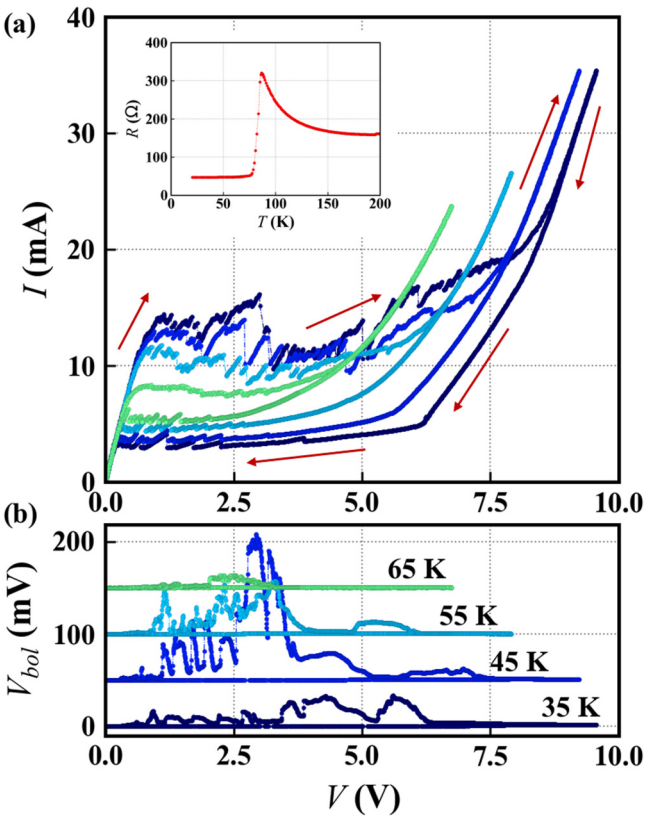

FIG. 4. (a) Typical temperature dependencies of the IVCs and (b) the radiation intensities detected by the HEB. V_{bol} is plotted as a function of the applied voltage to the Bi-chip-N_2. The data of V_{bol} are shifted vertically with 50 mV. The inset of the upper panel displays temperature dependencies of the *c*-axis resistivity. The temperature attached to the data indicates T_B of the sample.

after removing the metal deposited top surface of the crystal by cleaving, the low-angle side peak disappeared as displayed in Fig. 3. The slight change in the shape and position of the main peak may be due to the fact that the sample is larger than the x-ray beam diameter, causing the x-ray irradiation point on the sample to be slightly altered during the second sample setting.

This result strongly suggests that the origin of the low-angle side peak is due to processing treatment, such as deposition. Evaporation and sputtering are performed under a vacuum. Therefore, the crystal surfaces are prone to a decrease in oxygen concentration. This feature is observed as two peaks in the θ–2θ scan.

Figure 4(a) shows current–voltage characteristics (IVCs) of the Bi-chip-N_2 measured at various bath temperatures T_B. The voltage is low when the current starts to ramp up, and then when the applied current exceeds the critical Josephson current, I_c, it suddenly jumps to a large value, indicating that the system turns to the voltage state. Then, when the current is reduced, the voltage state persists down to a certain value of the current, thus forming a hysteresis loop as indicated by the arrows in Fig. 4. At 35 K, I_c is ~15 mA, and the maximum applied bias voltage V_c is ~7 V. According to the size of Bi-chips, the estimated J_c is ~0.14 kA/cm^2. As seen in Fig. 4(a), the hysteresis loop shrinks with increasing T_B.

In Fig. 4(b), the radiation intensities detected by the HEB (V_{bol}) are plotted as a function of the applied voltage to the Bi-chip-N_2. These data were obtained at the same time during the measurement of the IVCs shown in Fig. 4(a). EM waves are observed in the low current region of the IVCs from T_B = 35–65 K, with strong radiant intensity observed at T_B = 45 K. According to the previous studies, the maximum emission power observed here is estimated to be about a few μW. The observed results are consistent with the trends in device characteristics from previous studies.[27,29,31,54]

Figure 5(a) shows the IVC of the Bi-chip-O_2 observed between T_B ~ 35 K and 85 K. In the case of Bi-chip-O_2, IVCs exhibit large hysteresis loops along the current direction. For example, I_c and V_c at 35 K are ~40 mA and ~3 V, respectively. From the value of I_c, J_c can be estimated to be ~0.30 kA/cm^2. The hysteresis loops shrink rapidly with increasing T_B. At 70 K, a single hysteresis loop is observed at ~30 mA. Notably, at 75 K, a second hysteresis loop appears at ~80 mA. This result suggests not only the existence of crystal inhomogeneity in the Bi-chip-O_2 but also the existence of the two junctions with different I_c's.

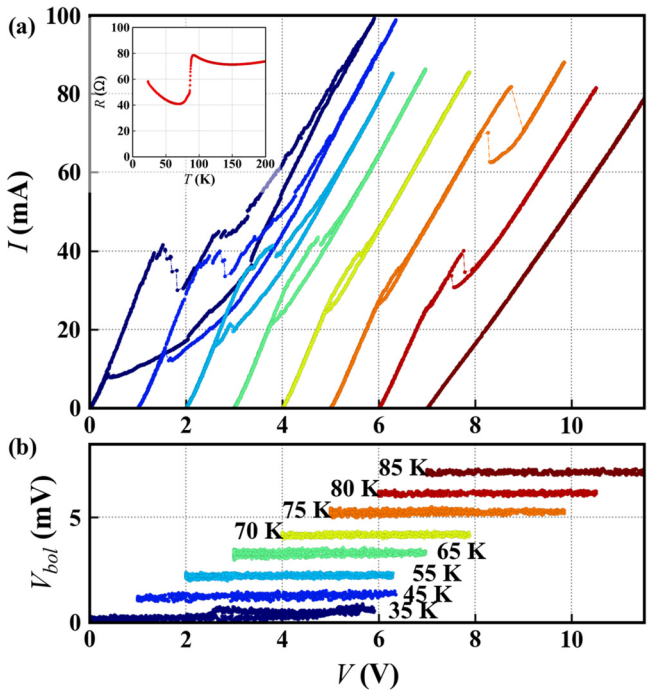

FIG. 5. (a) IVCs and (b) the bias voltage dependence of radiation intensities for the Bi-chip-O_2 observed from 35 to 85 K. Note that the data of the IVCs and V_{bol} are shifted horizontally with 1 V to understand the change of IVCs with increasing temperatures. The inset of the upper panel displays the temperature dependence of the *c*-axis resistivity.

The J_c's observed at lower temperatures are higher than that of Bi-chip-N_2. The increase in J_c observed for over-doped crystals seems to be consistent with previous studies.[55–57] However, the obtained value of J_c is one order of magnitude smaller than that of the over-doped crystals.[56,58] Therefore, the second hysteresis at ~80 mA ($J_c \sim 0.62$ kA/cm^2) appeared around 75 K is likely to have originated from the over-doped phase of the sample. This point will be discussed later.

Figure 5(b) shows the bias voltage dependence of the radiant intensity of the Bi-chip-O_2. As distinct from Bi-chip-N_2, apparent radiation was not observed. The device characteristics of Bi-chip-O_2 are completely different from those observed in the Bi-chip-N_2 in terms of the shape and size of the hysteresis loops, as well as the EM radiation capability. As for IVC at low temperatures, Bi-chip-N_2 has a lower I_c and a larger V_c, whereas Bi-chip-O_2 has a higher I_c and a smaller V_c.

The insets in Figs. 4(a) and 5(a) show the temperature dependence of the *c*-axis resistance. In both cases, the *c*-axis resistance shows an upturn from room temperature to low temperatures, with significant drops at about 85 K, which correspond to the superconducting transitions. The finite resistance below T_c is primarily attributed to the resistance of the thin film on the sapphire substrate, which serves as the power feed path, and the contact resistance measured by the two-terminal method. Therefore, the increase in resistivity near T_c in Bi-chip-O_2 includes the effect of contact resistance. Taking this into account, the resistivity upturn of Bi-chip-O_2 was much smaller than that of Bi-chip-N_2. This also confirms that Bi-chip-O_2 is more hole-doped.[45,46,50]

Here, we discuss the relationship between the crystals and the device characteristics based on the above experimental results. First, our annealing conditions clearly change the amount of hole-doping p of the crystals as shown in Fig. 1. According to the transition temperatures of the samples and Tallon's rule,[59] these are estimated to be $p \sim 0.134$ (N_2-annealed) and $p \sim 0.188$ (O_2-annealed). These correspond to so-called under-doped and over-doped samples.

The fabricated Bi-chips using those crystals clearly show a change in the *c*-axis lattice constants depending on the difference in hole-doping of the samples as seen in Fig. 2. As with the previous studies,[50,51] the *c*-axis lattice constant of Bi2212 shrinks with increasing oxygen content. In addition to the change in the lattice constant, the data obtained from θ–2θ scans clearly indicate the existence of the two crystalline layers with different lattice constants in the Bi-chip-O_2, while the Bi-chip-N_2 is expected to have a single domain. It means that the two layers would have different hole-doping.

As seen in Fig. 3, the separation of the peaks would be originated from the deposition processes of the metallic thin films by evaporation. For the deposition of the metallic thin films, small pieces of Au and Ag are heated in boats under a vacuum. The condition affects the surface of the crystals. In particular, the surface of O_2-annealed crystals would be highly sensitive and easily reduced during evaporation.

These characteristics are clearly reflected in the IVCs of the Bi-chips. In the case of the Bi-chip-N_2, a temperature-dependent single hysteresis loop is observed due to the single domain of the sample, as discussed in the θ–2θ scan data. The observed $J_c \sim 0.14$ kA/cm^2 at 35 K is comparable to that of previous studies. For example, Ozyuzer *et al.*[43] reported a value of 0.04–0.17 kA/cm^2 (at 12 K) for the under-doped crystal in the terahertz devices.

For the case of the Bi-chip-O_2, a single hysteresis loop of IVCs with $I_c \sim 40$ mA (estimated $J_c \sim 0.3$ kA/cm^2) is observed around 35 K. In addition, the two hysteresis loops in the IVCs are observed at higher T_B. As discussed in the θ–2θ scan data, these two hysteresis loops would be originated from the surface and inside parts of the Bi-chips. The surface part would have a smaller J_c compared to the inside part of the sample, as J_c generally increases exponentially with an increase in hole-doping.[55–58]

The observed $J_c \sim 0.3$ kA/cm^2 at 35 K is comparable to previous studies in which 0.36 kA/cm^2 (at 4.2 K) for the over-doped crystal[43] and 0.22 kA/cm^2 (at 70 K) for optimally doped crystals[52] have been reported. However, these J_c's are one order of magnitude smaller than the reported values, such as 2 kA/cm^2 at $p = 0.16$, 4.69 kA/cm^2 at $p = 0.186$, and 8 kA/cm^2 at $p = 0.19$.[56,58] The discrepancy of J_c's between our results and the previous studies[56,58] would be related to the preparation of the over-doped crystals. In our samples, as mentioned above, the carrier contents of the surface of the Bi-chip would be reduced by evaporation. This part has a small J_c; however, the inside of the Bi-chip has larger J_c's. At least, the inside part of the Bi-chip has $J_c \sim 0.62$ kA/cm^2 at 75 K. In addition, as seen in the IVCs from 85 to 75 K in Fig. 5, the value

of J_c of the inside part increases rapidly as T_bs decreases. Thus, the J_c of the inside part of the Bi-chip is even larger at low temperatures. The J_c would be similar to the previously reported values[56,58] at lower temperatures. It is noted that in the case of the Bi2212 THz device structures, the self-heating due to the application of dc bias voltage/current would be reflected in the reduction of the value of J_cs.

Finally, we discuss the emission characteristics of the devices. According to the x-ray peak intensity ratio for the Bi-chip-O_2, the volume fraction of the less doped layers corresponding to the surface part of the Bi-chip is small. At 35 K, these layers may meet the voltage conditions for terahertz radiation; however, the small volume fraction may be the most significant reason for the lack of clear emission from the sample. In addition, at high temperatures, the highly doped layers are also in a voltage state, but terahertz radiation was not observed here because the applied bias voltage to the sample was small relative to the fundamental oscillation conditions determined by the chip width.

On the other hand, the Bi-chip-N_2 is expected to be homogeneous crystalline characteristics from the θ–2θ scans as seen in Fig. 2. In fact, the IVCs of the sample have single hysteresis loops with lower I_c's compared to the Bi-chip-O_2. As shown in Fig. 4, clear THz radiation was observed from the sample since the whole IJJs of the Bi-chip-N_2 would contribute to the radiation.

As discussed above, a part of the device characteristics can be explained from a material perspective. While we need further work on device characteristics related to the hole-doping of the crystals, the relationships among hole-doping, lattice constants, and IVCs can be understood. In addition, it is evident that the surface of the over-doped crystals is very sensitive to the heat treatment processes, such as electrode evaporation on the crystal surface. This information is important for preparing the crystals for the THz emitting devices.

IV. CONCLUSIONS

The device characteristics of Bi2212-THz emitters were analyzed based on the properties of the crystal. Bi2212 single crystals annealed under N_2 and O_2 gas flow were fabricated into Bi-chips by the wet etching method. X-ray diffraction was performed on the chips to investigate the difference in the *c*-axis lattice constant with respect to the excess oxygen content. As a result, it was found that only in O_2-annealed crystals, the excess oxygen near the chip surface is reduced by metal deposition. This change in the lattice constant corresponds well to the difference in J_c's in device properties, especially reflected in the two hysteresis loops on the IVC of the O_2-annealed sample. This understanding of the crystal properties also offers a reasonable explanation for why clear emission was only obtained from the N_2-annealed sample. The results of this study reveal processing issues in Bi2212 single crystals with high oxygen content and provide useful information for the development of Bi2212-THz emitters.

ACKNOWLEDGMENTS

This study was supported by the Japan Society for the Promotion of Science Grant-in-Aid for Scientific Research (No. 15H01996). T.K. was supported by the Japan Society for the Promotion of Science Grant-in-Aid for Scientific Research (Nos. 17K05018 and 20H02590). This study was also supported by TIA-Kakehashi grants (Nos. 2018-43 and 2019-47). The x-ray diffraction measurements were performed under the approval of the Photon Factory Program Advisory Committee (Proposal No. 2019G634).

AUTHOR DECLARATIONS

Conflict of Interest

The authors have no conflicts to disclose.

Author Contributions

S. Nakagawa: Conceptualization (equal); Data curation (equal); Formal analysis (equal); Investigation (lead); Visualization (lead); Writing – original draft (lead); Writing – review & editing (lead). **T. Shizu:** Formal analysis (equal); Investigation (equal). **T. Imai:** Investigation (equal). **M. Nakayama:** Investigation (equal). **J. Kim:** Investigation (equal). **H. Minami:** Resources (equal); Writing – review & editing (equal). **K. Kadowaki:** Resources (equal); Writing – review & editing (equal). **M. Tsujimoto:** Writing – review & editing (equal). **H. Nakao:** Investigation (supporting); Methodology (equal); Software (equal); Supervision (equal); Writing – review & editing (equal). **H. Eisaki:** Supervision (equal); Writing – original draft (equal); Writing – review & editing (equal). **S. Ishida:** Writing – review & editing (equal). **T. Mochiku:** Writing – review & editing (equal). **Y. Hasagawa:** Writing – review & editing (equal). **T. Kashiwagi:** Conceptualization (equal); Data curation (equal); Funding acquisition (equal); Investigation (equal); Project administration (equal); Resources (equal); Supervision (equal); Writing – original draft (lead); Writing – review & editing (lead).

DATA AVAILABILITY

The data that support the findings of this study are available within the article.

REFERENCES

[1]M. Tonouchi, "Cutting-edge terahertz technology," Nat. Photonics **1**, 97–105 (2007).
[2]B. Ferguson and X.-C. Zhang, "Materials for terahertz science and technology," Nat. Mater. **1**, 26–33 (2002).
[3]S. Dhillon, M. Vitiello, E. Linfield, A. Davies, M. C. Hoffmann, J. Booske, C. Paoloni, M. Gensch, P. Weightman, G. Williams, and E. Castro-Camus, "The 2017 terahertz science and technology roadmap," J. Phys. D: Appl. Phys. **50**, 043001 (2017).
[4]Y. Koyama, R. Sekiguchi, and T. Ouchi, "Oscillations up to 1.40 THz from resonant-tunneling-diode-based oscillators with integrated patch antennas," Appl. Phys. Express **6**, 064102 (2013).
[5]M. Asada and S. Suzuki, "Room-temperature oscillation of resonant tunneling diodes close to 2 THz and their functions for various applications," J. Infrared Millim. Terahertz Waves **37**, 1185–1198 (2016).
[6]S. Suzuki, M. Shiraishi, H. Shibayama, and M. Asada, "High-power operation of terahertz oscillators with resonant tunneling diodes using impedance-matched antennas and array configuration," IEEE J. Sel. Top. Quantum Electron. **19**, 8500108 (2012).

[7]M. Feiginov, "Frequency limitations of resonant-tunnelling diodes in sub-THz and THz oscillators and detectors," J. Infrared Millim. Terahertz Waves **40**, 365–394 (2019).
[8]B. S. Williams, "Terahertz quantum-cascade lasers," Nat. Photonics **1**, 517–525 (2007).
[9]B. S. Williams, S. Kumar, Q. Hu, and J. L. Reno, "High-power terahertz quantum-cascade lasers," Electron. Lett. **42**, 89–91 (2006).
[10]C. Walther, M. Fischer, G. Scalari, R. Terazzi, N. Hoyler, and J. Faist, "Quantum cascade lasers operating from 1.2 to 1.6 THz," Appl. Phys. Lett. **91**, 131122 (2007).
[11]S. Fathololoumi, E. Dupont, C. Chan, Z. Wasilewski, S. Laframboise, D. Ban, A. Mátyás, C. Jirauschek, Q. Hu, and H. Liu, "Terahertz quantum cascade lasers operating up to 200 K with optimized oscillator strength and improved injection tunneling," Opt. Express **20**, 3866–3876 (2012).
[12]J. Kiessling, I. Breunig, P. Schunemann, K. Buse, and K. Vodopyanov, "High power and spectral purity continuous-wave photonic THz source tunable from 1 to 4.5 THz for nonlinear molecular spectroscopy," New J. Phys. **15**, 105014 (2013).
[13]H. Kanaya, R. Sogabe, T. Maekawa, S. Suzuki, and M. Asada, "Fundamental oscillation up to 1.42 THz in resonant tunneling diodes by optimized collector spacer thickness," J. Infrared Millim. Terahertz Waves **35**, 425–431 (2014).
[14]S. Suzuki, M. Asada, A. Teranishi, H. Sugiyama, and H. Yokoyama, "Fundamental oscillation of resonant tunneling diodes above 1 THz at room temperature," Appl. Phys. Lett. **97**, 242102 (2010).
[15]T. Maekawa, H. Kanaya, S. Suzuki, and M. Asada, "Oscillation up to 1.92 THz in resonant tunneling diode by reduced conduction loss," Appl. Phys. Express **9**, 024101 (2016).
[16]Y. Jiang, K. Vijayraghavan, S. Jung, A. Jiang, J. H. Kim, F. Demmerle, G. Boehm, M. C. Amann, and M. A. Belkin, "Spectroscopic study of terahertz generation in mid-infrared quantum cascade lasers," Sci. Rep. **6**, 21169 (2016).
[17]K. Fujita, S. Jung, Y. Jiang, J. H. Kim, A. Nakanishi, A. Ito, M. Hitaka, T. Edamura, and M. A. Belkin, "Recent progress in terahertz difference-frequency quantum cascade laser sources," Nanophotonics **7**, 1795–1817 (2018).
[18]Q. Lu, D. Wu, S. Sengupta, S. Slivken, and M. Razeghi, "Room temperature continuous wave, monolithic tunable THz sources based on highly efficient mid-infrared quantum cascade lasers," Sci. Rep. **6**, 23595 (2016).
[19]R. Kleiner, F. Steinmeyer, G. Kunkel, and P. Müller, "Intrinsic Josephson effects in $Bi_2Sr_2CaCu_2O_8$ single crystals," Phys. Rev. Lett. **68**, 2394 (1992).
[20]R. Kleiner and P. Müller, "Intrinsic Josephson effects in high-T_c superconductors," Phys. Rev. B **49**, 1327 (1994).
[21]A. Yurgens, "Intrinsic Josephson junctions: Recent developments," Supercond. Sci. Technol. **13**, R85 (2000).
[22]L. Ozyuzer, A. E. Koshelev, C. Kurter, N. Gopalsami, Q. Li, M. Tachiki, K. Kadowaki, T. Yamamoto, H. Minami, H. Yamaguchi, and T. Tachiki, "Emission of coherent THz radiation from superconductors," Science **318**, 1291–1293 (2007).
[23]B. Josephson, "Tunneling into superconductors," Phys. Lett. **1**, 251 (1962).
[24]H. Minami, I. Kakeya, H. Yamaguchi, T. Yamamoto, and K. Kadowaki, "Characteristics of terahertz radiation emitted from the intrinsic Josephson junctions in high-T_c superconductor $Bi_2Sr_2CaCu_2O_{8+\delta}$," Appl. Phys. Lett. **95**, 232511 (2009).
[25]K. Kadowaki, M. Tsujimoto, K. Yamaki, T. Yamamoto, T. Kashiwagi, H. Minami, M. Tachiki, and R. A. Klemm, "Evidence for a dual-source mechanism of terahertz radiation from rectangular mesas of single crystalline $Bi_2Sr_2CaCu_2O_{8+\delta}$ intrinsic Josephson junctions," J. Phys. Soc. Jpn. **79**, 023703 (2010).
[26]M. Tsujimoto, K. Yamaki, K. Deguchi, T. Yamamoto, T. Kashiwagi, H. Minami, M. Tachiki, K. Kadowaki, and R. A. Klemm, "Geometrical resonance conditions for THz radiation from the intrinsic Josephson junctions in $Bi_2Sr_2CaCu_2O_{8+\delta}$," Phys. Rev. Lett. **105**, 037005 (2010).
[27]T. Kitamura, T. Kashiwagi, T. Yamamoto, M. Tsujimoto, C. Watanabe, K. Ishida, S. Sekimoto, K. Asanuma, T. Yasui, K. Nakade, and Y. Shibano, "Broadly tunable, high-power terahertz radiation up to 73 K from a stand-alone $Bi_2Sr_2CaCu_2O_{8+\delta}$ mesa," Appl. Phys. Lett. **105**, 202603 (2014).
[28]T. Kashiwagi, K. Sakamoto, H. Kubo, Y. Shibano, T. Enomoto, T. Kitamura, K. Asanuma, T. Yasui, C. Watanabe, K. Nakade, and Y. Saiwai, "A high-T_c intrinsic Josephson junction emitter tunable from 0.5 to 2.4 terahertz," Appl. Phys. Lett. **107**, 082601 (2015).
[29]T. Kashiwagi, T. Yamamoto, T. Kitamura, K. Asanuma, C. Watanabe, K. Nakade, T. Yasui, Y. Saiwai, Y. Shibano, H. Kubo, and K. Sakamoto, "Generation of electromagnetic waves from 0.3 to 1.6 terahertz with a high-T_c superconducting $Bi_2Sr_2CaCu_2O_{8+\delta}$ intrinsic Josephson junction emitter," Appl. Phys. Lett. **106**, 092601 (2015).
[30]M. Ji, J. Yuan, B. Gross, F. Rudau, D. An, M. Li, X. Zhou, Y. Huang, H. Sun, Q. Zhu, and J. Li, "$Bi_2Sr_2CaCu_2O_8$ intrinsic Josephson junction stacks with improved cooling: Coherent emission above 1 THz," Appl. Phys. Lett. **105**, 122602 (2014).
[31]D. An, J. Yuan, N. Kinev, M. Li, Y. Huang, M. Ji, H. Zhang, Z. Sun, L. Kang, B. Jin, and J. Chen, "Terahertz emission and detection both based on high-T_c superconductors: Towards an integrated receiver," Appl. Phys. Lett. **102**, 092601 (2013).
[32]S. Sekimoto, C. Watanabe, H. Minami, T. Yamamoto, T. Kashiwagi, R. A. Klemm, and K. Kadowaki, "Continuous 30 μw terahertz source by a high-T_c superconductor mesa structure," Appl. Phys. Lett. **103**, 182601 (2013).
[33]T. Benseman, K. Gray, A. Koshelev, W.-K. Kwok, U. Welp, H. Minami, K. Kadowaki, and T. Yamamoto, "Powerful terahertz emission from $Bi_2Sr_2CaCu_2O_{8+\delta}$ mesa arrays," Appl. Phys. Lett. **103**, 022602 (2013).
[34]E. A. Borodianskyi and V. M. Krasnov, "Josephson emission with frequency span 1–11 THz from small $Bi_2Sr_2CaCu_2O_{8+\delta}$ mesa structures," Nat. Commun. **8**, 1742 (2017).
[35]A. Elarabi, Y. Yoshioka, M. Tsujimoto, and I. Kakeya, "Monolithic superconducting emitter of tunable circularly polarized terahertz radiation," Phys. Rev. Appl. **8**, 064034 (2017).
[36]A. Elarabi, Y. Yoshioka, M. Tsujimoto, and I. Kakeya, "Circularly polarized terahertz radiation monolithically generated by cylindrical mesas of intrinsic Josephson junctions," Appl. Phys. Lett. **113**, 052601 (2018).
[37]M. Tsujimoto, S. Fujita, G. Kuwano, K. Maeda, A. Elarabi, J. Hawecker, J. Tignon, J. Mangeney, S. S. Dhillon, and I. Kakeya, "Mutually synchronized macroscopic Josephson oscillations demonstrated by polarization analysis of superconducting terahertz emitters," Phys. Rev. Appl. **13**, 051001 (2020).
[38]U. Welp, K. Kadowaki, and R. Kleiner, "Superconducting emitters of THz radiation," Nat. Photonics **7**, 702–710 (2013).
[39]I. Kakeya and H. Wang, "Terahertz-wave emission from Bi2212 intrinsic Josephson junctions: A review on recent progress," Supercond. Sci. Technol. **29**, 073001 (2016).
[40]T. Kashiwagi, H. Kubo, K. Sakamoto, T. Yuasa, Y. Tanabe, C. Watanabe, T. Tanaka, Y. Komori, R. Ota, G. Kuwano, and K. Nakamura, "The present status of high-T_c superconducting terahertz emitters," Supercond. Sci. Technol. **30**, 074008 (2017).
[41]R. Kleiner and H. Wang, "Terahertz emission from $Bi_2Sr_2CaCu_2O_{8+x}$ intrinsic Josephson junction stacks," J. Appl. Phys. **126**, 171101 (2019).
[42]K. Delfanazari, R. A. Klemm, H. J. Joyce, D. A. Ritchie, and K. Kadowaki, "Integrated, portable, tunable, and coherent terahertz sources and sensitive detectors based on layered superconductors," Proc. IEEE **108**, 721–734 (2020).
[43]L. Ozyuzer, Y. Simsek, H. Koseoglu, F. Turkoglu, C. Kurter, U. Welp, A. E. Koshelev, K. E. Gray, W. Kwok, T. Yamamoto, and K. Kadowaki, "Terahertz wave emission from intrinsic Josephson junctions in high-T_c superconductors," Supercond. Sci. Technol. **22**, 114009 (2009).
[44]T. Mochiku and K. Kadowaki, "Growth and properties of $Bi_2Sr_2(Ca,Y)Cu_2O_{8+\delta}$ single crystals," Phys. C: Supercond. **235**, 523–524 (1994).
[45]Y. Idemoto and K. Fueki, "Oxygen nonstoichiometry and valences of bismuth and copper in $Bi_{2.00}Sr_{1.88}Ca_{1.00}Cu_{2.14}O_y$," Phys. C: Supercond. **168**, 167–172 (1990).

[46]T. Watanabe, T. Fujii, and A. Matsuda, "Anisotropic resistivities of precisely oxygen controlled single-crystal $Bi_2Sr_2CaCu_2O_{8+\delta}$: Systematic study on"spin gap" effect," Phys. Rev. Lett. **79**, 2113 (1997).
[47]Y. Shibano, T. Kashiwagi, Y. Komori, K. Sakamoto, Y. Tanabe, T. Yamamoto, H. Minami, R. A. Klemm, and K. Kadowaki, "High-T_c superconducting THz emitters fabricated by wet etching," AIP Adv. **9**, 015116 (2019).
[48]T. Imai, T. Kashiwagi, S. Nakagawa, M. Nakayama, J. Kim, G. Kuwano, M. Tsujimoto, H. Minami, and K. Kadowaki, "Investigation of wet etching solutions and method for thicker stand alone type of mesa structures of Bi2212 single crystals," Jpn. J. Appl. Phys. **60**, 126501 (2021).
[49]T. Kashiwagi, T. Yuasa, Y. Tanabe, T. Imai, G. Kuwano, R. Ota, K. Nakamura, Y. Ono, Y. Kaneko, M. Tsujimoto, and H. Minami, "Improved excitation mode selectivity of high-T_c superconducting terahertz emitters," J. Appl. Phys. **124**, 033901 (2018).
[50]Y. Kotaka, T. Kimura, H. Ikata, J. Shimoyama, K. Kitazawa, K. Yamafuji, K. Kishio, and D. Pooke, "Doping state and transport anisotropy in Bi2212 single crystals," Phys. C: Supercond. **235**, 1529–1530 (1994).
[51]J.-Y. Genoud, G. Triscone, A. Junod, T. Tsukamoto, and J. Muller, "Reversible magnetization as a function of the oxygen concentration in Bi-2212 superconducting ceramics," Phys. C: Supercond. **242**, 143–154 (1995).
[52]X. Sun, W. Wu, L. Zheng, X. Zhao, L. Shi, G. Zhou, X.-G. Li, and Y. Zhang, "Effects of oxygen doping and structural distortion on the superconductivity of $Bi_2Sr_2CaCu_2O_y$ single crystals," J. Phys.: Condens. Matter **9**, 6391 (1997).
[53]A. Baker and B. Glowacki, "The effect of Bi content on the phase purity and the superconducting critical temperature of a Sr and Ca deficient Bi-2212 stoichiometry," Phys. C: Supercond. **227**, 31–39 (1994).
[54]K. Kadowaki, M. Tsujimoto, K. Delfanazari, T. Kitamura, M. Sawamura, H. Asai, T. Yamamoto, K. Ishida, C. Watanabe, S. Sekimoto, and K. Nakade, "Quantum terahertz electronics (QTE) using coherent radiation from high temperature superconducting $Bi_2Sr_2CaCu_2O_{8+\delta}$ intrinsic Josephson junctions," Phys. C: Supercond. **491**, 2–6 (2013).
[55]Y. Yamada, K. Anagawa, T. Shibauchi, T. Fujii, T. Watanabe, A. Matsuda, and M. Suzuki, "Interlayer tunneling spectroscopy and doping-dependent energy-gap structure of the trilayer superconductor $Bi_2Sr_2Ca_2Cu_3O_{10+\delta}$," Phys. Rev. B **68**, 054533 (2003).
[56]M. Suzuki, T. Hamatani, K. Anagawa, and T. Watanabe, "Evolution of interlayer tunneling spectra and superfluid density with doping in $Bi_2Sr_2CaCu_2O_{8+\delta}$," Phys. Rev. B **85**, 214529 (2012).
[57]H. Kambara, I. Kakeya, and M. Suzuki, "Increase of superfluid density with growth of quasiparticle density of states probed by intrinsic tunneling spectroscopy in $Bi_{1.9}Pb_{0.1}Sr_2CaCu_2O_{8+\delta}$," Phys. Rev. B **87**, 214521 (2013).
[58]T. Jacobs, Y. Simsek, Y. Koval, P. Müller, and V. M. Krasnov, "Sequence of quantum phase transitions in $Bi_2Sr_2CaCu_2O_{8+\delta}$ cuprates revealed by in situ electrical doping of one and the same sample," Phys. Rev. Lett. **116**, 067001 (2016).
[59]J. L. Tallon, C. Bernhard, H. Shaked, R. Hitterman, and J. Jorgensen, "Generic superconducting phase behavior in high-T_c cuprates: T_c variation with hole concentration in $YBa_2Cu_3O_{7-\delta}$," Phys. Rev. B **51**, 12911 (1995).